NUMERICAL SIMULATION FOR EVALUATING CHILD OCCUPANT BEHAVIOUR IN THE CASE OF A REAR IMPACT

Marius-Dorin Surcel
FPInnovations
Marius-Petrino Buzatu
Aurelian Vadean
École Polytechnique de Montréal
Canada
Paper Number 09-0029

ABSTRACT

This project uses dynamic simulations to assess the effectiveness of child restraint systems in the case of rear impact, in various installation configurations and for different acceleration pulses.
The model was mainly based on a multi-body method, using the MADYMO software. However, the side wings of the child restraint system have been modelled by the finite-element technique, to ensure a better representation of the contacts between the child dummy and the restraining device.
The study shows that the neck is the most exposed part of the body and in some situations the neck injury criteria overpass the limit values. Thus, the case of the neck injury criteria in tension-extension for the installation using vehicle safety belts, when the result is more than double than the limit value.
The simulations employed two triangular pulses, with speed variation of 16 km/h and 25 km/h, and one trapezoidal pulse, with speed variation of 25 km/h. In all cases, the results are proportional with the speed variation. Furthermore, the two triangular pulses give higher values for injury criteria than the trapezoidal pulse.
Installation of a child restraint using rigid anchorages and lower straps offers the best protection for the child passenger in the case of rear-end collision. The acceleration pulse is a crucial factor for the accuracy of tests and the realism of simulations.
The principal limitation of the study refers to the injury criteria that are not yet well defined and for which does not exist a consensus in the case of a rear impact.
The paper presents an approach for simulating rear-end collision involving child passengers, which could be used for comparative studies of different rear-impact scenarios, such as different acceleration pulses or installations.

INTRODUCTION

Real life accident data are showing that the slow-speed rear-impact can produce neck injury causing invalidity and long-term disability. These injuries, abbreviated WAD (Whiplash Associated Disorders) are usually classified as AIS 1 (Hynd and van Ratingen, 2005). AIS – Abbreviated Injury Scale, created by The Association for the Advancement of Automotive Medicine (AAAM), is the most used injury classification scale, where 0 signifies that there is no injury and 6 designates unsurvivable injuries.
A study conducted in Japan and presented by Sawada and Hasegawa (2005) showed that neck injury represent around eighty percent from the total injuries caused by rear-end accidents. According to Fatality Analysis Reporting System - FARS (NHTSA, 2002), in the USA in 1999, 8 % of the children (101 children) killed in road accidents were involved in rear-end accidents. Between 1991 and 2000, in USA, 662 children were killed in rear-end accidents, representing 7 % of the total number of the children dead in traffic accidents in the considered period. More than 30 % of these victims (214) were seated in a child restraint system during the accident (NHTSA, 2004).
In Quebec in 1987, $18 millions was paid for damages caused by this type of accident, which determined La Société d'Assurance d'Automobile du Québec (SAAQ) to form a special workgroup, Quebec Task Force, with a view to studying the injuries produced by whiplash (Spitzer et al., 1995). This study is considered the reference for similar research (Freeman et al., 1998 and Versteegen et al., 2001).
Boyd et al. (2008) present a study performed in England for eight months in emergency rooms, which used the Québec Task Force methodology. The study identified 101 child passengers victims of rear-end accidents, from which 49 (47 %) were presenting WAD symptoms. The average duration of the symptoms was 8.8 days, showing more important incidence than in similar studies.
In order to assess the emergency of having rear impact regulatory stipulations for child passenger protection, NHTSA performed some dynamic sled tests at both 17.5 and 30.5 km/h impact speeds using a CRABI 12-month-old dummy. The dummy, seated in an Evenflo On My Way rear-facing infant seat, was installed on the rear seat of a 1999 Dodge

Intreprid vehicle body. Because the measured injury parameters did not exceed the limits stipulated by FMVSS 208 and considering that a 7 % fatality is low, it was concluded that it is not necessary yet to stipulate special requirements for the child passenger protection in the case of rear impact (NHTSA, 2004). According to Croft (2000), the risk for a child passenger represents two-thirds of the risk for an adult occupant but despite this high risk, less than 2 % of rear-end impact studies are dedicated to child passenger protection.

Another element of importance for studying WAD associated to child occupant, presented by Klinich et al. (1996), is the fact that the weight of the head of the child is proportionally more important with respect to the rest of the body than for the adult, one forth compared with one seventh, thus favouring the lesions of the spine.

While the efficiency of child restraint systems was very well proven in frontal collisions, and studies regarding side impact collisions are continually increasing, the performances of these devices in the case of a rear-end collision were not yet sufficiently demonstrated. The objective of the project presented in this paper was to study by simulation the behaviour of the child dummy in the case of a rear-end impact, for various acceleration pulses and in different installation configurations of the child restraint system.

METHODOLOGY

General Approach

The first step of the project stands for the development of the model. The study is based on multi-body method but the side wings of the child restraint system have been modelled by the finite-element technique. This modelling allows for a better representation of the contacts between the child dummy and the restraining device. The second step, consisting in model exploitation, presents rear-end impact simulations for different acceleration pulses and in various installation configurations of the child restraint system.

Child Dummy

The majority of the studies on the effect of the impact on child passengers use three-years-old child dummies. Adult rear-impact dummy models are available in MADYMO Data Base, such are Hybrid III – TRID Neck (Hybrid III dummy with the neck model adapted for rear impact), RID II and BioRid II, but there is not yet any child dummy specially destined for the study of rear impact. The model on which this study is based uses the Hybrid III – 3-years-old child dummy (Surcel, 2004). The Hybrid III series was designed for front impact studies, thus the accuracy of the evaluation of the risk in the case of a rear impact was not yet verified by experimental studies. According to European Vehicle Passive Safety Network 2 (2004), because their neck mimics human bending response in flexion and extension, these dummies can be used in rear as well as frontal collision evaluations.

In spite of the above mentioned limitations, we have chosen for our model a Hybrid III – 3-years-old child dummy model, consisting of 28 ellipsoids while certain head regions are built using finite elements. The contact between head and thorax is defined by default. Additional contacts have been defined to consider the interactions between different parts of the model: between femurs; between each femur and the abdomen, the thorax, the neck and the head; between tibias; between each tibia, the neck, and the head; between arms; between each arm, the neck and the head.

Models

For the chosen child dummy model, the required child seat is the convertible restraint system designed for use by infants and toddlers. The child seat model described by Surcel and Gou (2005) was used. It is made of a shell and its support that is in contact with the vehicle bench cushion. A padding that satisfies energy absorption requirements covers the inside of the shell. A contact stiffness function was defined for the padding of the child restraint system. The seat is also equipped with a tilting adjustment button, a rear support and a harness.

The central region of the child seat, consisting of sixty-eight ellipsoids and four cylinders, has been assembled with the side wings, modelled using finite elements in order to allow for a better representation of the contacts between the child dummy and the restraining device (Figure 1).

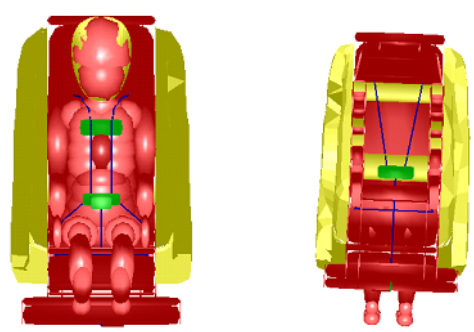

Figure 1. Installation of child restraint system harness.

The child restraint system can be installed using vehicle safety belts or the lower rigid anchorages and straps. The upper part of the seat back is attached to the vehicle's structure with a top tether.
The material properties for the child seat and the belts and straps characteristics are those used by Surcel (2004). All the straps were represented using MADYMO belt segments. The child restraint system attachments, vehicle safety belt anchorages and rigid anchorages were built by ellipsoids. Figure 2 present child seat installations.

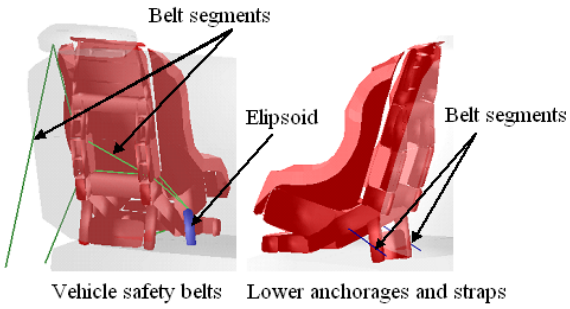

Figure 2. Child restraint system installation.

The test sled was modelled using ellipsoids, based on the description given in test method 213 (Transport Canada, 2001).). The contact stiffness for the sled bench cushion and sled bench back was defined by force-deflection curves. Figure 3 presents the model of the test sled.

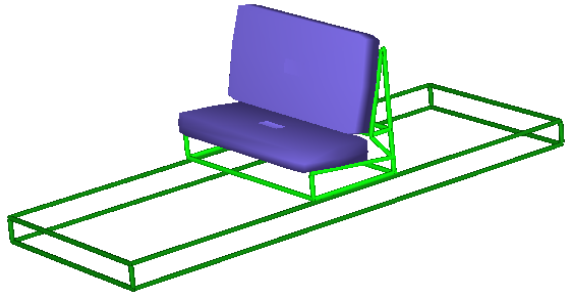

Figure 3. Test sled model.

The model on which is based this study was evaluated for side and frontal impact against similar test data. The simulation results were generally very close to experimental data (Surcel, 2004; Surcel and Gou, 2005). There are not enough accidentology studies and experimental data are practically inexistent for child passengers involved in a rear impact. Thus, validation of the model for rear impact or, at least, comparing the results of the simulations with test results was not possible.

Injury Criteria

Injury criteria are necessary in order to evaluate the risk for the passenger in case of an accident and for correlating the loading conditions during impact with the injury scales.
WAD-RAP (Whiplash Associated Disorders - Risk Assessment Parameters) is intended to replace injury criteria when the actual cause of the Whiplash Associated Disorders is not known. According to Hynd and Ratingen (2005), from the regulatory point of view, it is necessary to have a good correlation between WAD-RAP and the risk. This condition is fulfilled by the neck injury criteria (NIC) and by the Nkm criteria, which is based on a combination of shearing forces and bending moments in the upper neck (Schmitt et al., 2001). Another proposed combined criteria for evaluating neck injury in the case of a rear impact is LNL (Lower Neck Load), a combination of lower neck loading in shearing, tension and extension (Heitplatz et al., 2003).
Head Injury Criteria (HIC) is the most used criteria for evaluating the severity of the head injuries and it gives the necessary information to differentiate the contact impact response from the non-contact impact response. HIC is calculated based on « Wayne State Tolerance Curve » (WSTC) and it was established only for the front – to rear direction impact. In our case, contacts are defined between the head of the child dummy and the child seat back with the loading applied in a longitudinal direction. Therefore, we consider that the usage of HIC is appropriate for our study.
Other studies have shown that the neck forces and moments, as well as the head and the thorax acceleration, might not have an adequate biofidelty for the study of the rear impact. Consequently, the neck injury criteria NIC and Nij, which computation are based on the above mentioned parameters, might be also inadequate for the rear impact study (Kuppa et al., 2005).
The European Automobile Manufacturers' Association (ACEA) has carried out a study looking at the repeatability and reproducibility of the proposed test procedures and injury criteria for rear impact, using 16 km/h and 25 km/h – delta-V (ΔV) pulses (Adalian et al. 2005). The injury criteria used for the BioRID adult dummy were head, spine and pelvis accelerations, lower and upper neck forces and moments as well as the combined criteria LNL, Nkm and NIC, and the contacts between the seat and the dummy. The repeatability of most of the injury criteria at 16 km/h was acceptable but reproducibility was poor, with variations of up to 40% for some of the criteria. The situation worsened at 25 km/h, with some criteria yielding variations of over 100%. The

study concluded that the injury criteria must be very carefully selected, and the high severity pulses might be inadequate for neck injury assessment.
The linear and angular head accelerations and the head displacement are also used during the rear impact tests performed by insurance companies (GDV- Alianz-Germany) and research institutes (JARI - Japan Automobile Research Institute and TRI - Transport Research Institute – United Kingdom).
The actual injury, causing the typical WAD symptoms, and the injury mechanism are still unknown, though hypotheses exist. The evaluation of the currently proposed injury criteria, such as LNL, Nkm and NIC, is statistically derived from field accident data and reconstructions of real world accident situations (Hynd et van Ratingen, 2005). An important validation work is still necessary, and especially for the child passengers.
The fore mentioned considerations as well as the MADYMO output data availability, guide us on the choice of the parameters for evaluating the behaviour of the child dummy response in the case of the rear impact simulation. Table 1 presents these parameters.

Table 1.
Evaluation parameters

N°	Description	Symbol
1	Head Injury Criteria – 15 ms	HIC 15
2	Head Injury Criteria – 36 ms	HIC 36
3	Head Injury Criteria – unlimited	HIC
4	Thorax deflection	DT
5	Head linear acceleration in the centre of gravity, m/s^2	HCG_acc
6	Head angular acceleration, rad/s^2	Hang_acc
7	Thorax deceleration - 3ms, m/s^2	T3ms
8	Neck injury criteria in tension – extension	Nij TE
9	Neck injury criteria in tension – flexion	Nij TF
10	Neck injury criteria in compression – extension	Nij CE
11	Neck injury criteria in compression – flexion	Nij CF
12	Rearward neck injury criteria, m/s^2	NIC Rr
13	Resultant force in the lower neck, N	NLow_F
14	Resultant force in the upper neck, N	NUp_F
15	Resultant moment in lower neck, Nm	NLow_M
16	Resultant moment in upper neck, Nm	NUp_M

Acceleration Pulses and Simulations

WG20 working group has been set-up within EEVC (European Enhanced Vehicle Safety Committee) for studying the rear impact test procedures and rear impact neck injuries.
WG task is to develop sled test procedures in order to define acceleration pulses, installation and test dummies. Based on accident data records from several countries, WG20 reported that the majority of these types of injuries occur in medium impact severity crashes consisting in change of velocity (ΔV), between 10 and 15 km/h, and deceleration less than 4 g. These are short-term injury and the patients recover within a couple of weeks. Long-term injuries, with consequences lasting more than one month, are produced by impacts with ΔV greater than 20 km/h and deceleration more than 5 g (Hynd et van Ratingen, 2005). Consequently, the low severity accidents are well reproduced by using acceleration pulses with $\Delta V < 20$ km/h, while the impacts with more severe consequences are corresponding to acceleration pulses with $\Delta V \geq 20$ km/h. In order to study both situations, we chose one acceleration pulse with $\Delta V = 16$ km/h and two acceleration pulses with $\Delta V = 25$ km/h. Figure 4 presents these pulses, adapted from Sawada and Hasegawa (2005).
The acceleration pulse no. 1, used by IIWPG (International Insurance Whiplash Prevention) and ADAC (Allgemeiner Deutscher Automobil-Club e.V.), corresponds to $\Delta V = 16$ km/h. For $\Delta V = 25$ km/h we used the triangular acceleration pulse no. 2, also proposed by ADAC, and the trapezoidal acceleration pulse no. 3, adopted by the Swedish insurance company Folksam.

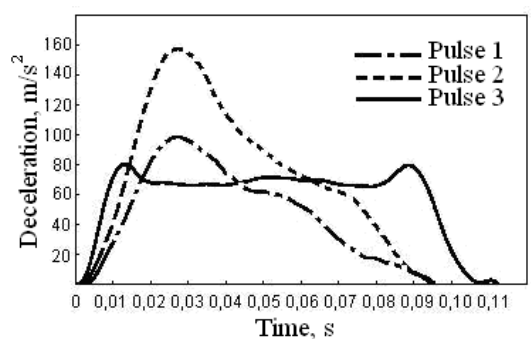

Figure 4. Acceleration pulses for rear impact, adapted from Sawada and Hasegawa (2005).

To simulate the rear impact, the rear acceleration field and the gravity field were applied to the child dummy and to the child restraint system. The study compared the results obtained with the three different acceleration pulses described above, and considered

the two different installation configurations - vehicle seat belts and lower anchorages and straps.
The results of the simulation were also compared with the Injury Assessment Reference Values (IARV), stipulated by FMVSS 208 and FMVSS 213, and with the reference values proposed by Klinch et al. (2006). These injury parameters are for frontal impact and may not accurately reflect the risk of injury in rear impact. The corresponding Injury Assessment Reference Values should be used for reference purposes only. For thorax acceleration, the two standards stipulate different values: 540 m/s^2 (FMVSS 208) and 589 m/s^2 (FMVSS 213).

RESULTS AND DISCUSSIONS

Comparison Study for Different Acceleration Pulses

This section presents the results of the simulations performed with the three different acceleration pulses with the child restraint system installed using the lower anchorages and straps. In all cases, the upper part of the child restraint system is attached to the vehicle body with a top tether while the child is attached with the harness provided by the child restraint system. Similar simulations have been conducted with CRS installed using vehicle's safety belts.
The simulation results show that both the child dummy and the child restraint system moved rearward under the action of the acceleration field. The vehicle safety belts and the child restrain harness were stressed and the child dummy entered into contact with the child seat back. The child dummy was pushed to the front by the reaction forces due to the impact with the back of the CRS and by the elastic forces in the harness and in the straps. Figure 5 illustrates the model during the simulation of the rear impact and Table 2 presents the results of the simulation.

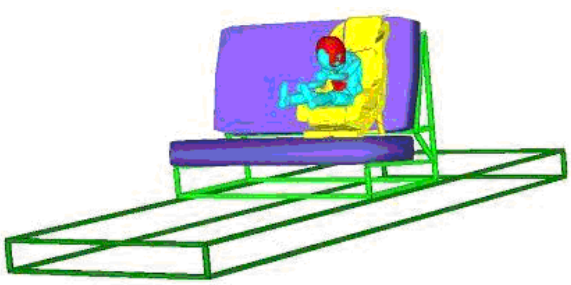

Figure 5. Rear impact simulation.

It can be observed that the acceleration pulse no. 2 (ΔV=25 km/h, triangular) generally gives higher values for the injury criteria than the two other pulses. The result for the neck injury criteria in tension – extension (Nij TE) is the only one exceeding the admissible value, with 12 %.

Table 2.
Injury criteria comparison for the simulations using the three acceleration pulses and the CRS installed with lower anchorages and straps

N^o	Parameter	Acceleration pulse			Ref. value
		1	2	3	
1	HIC 15	34	44	25	570
2	HIC 36	34	48	25	1000
3	HIC	49	84	37	1000
4	DT, mm	24	26	18	34
5	HCG_acc, m/s^2	354	501	325	785
6	Hang_acc, rad/s^2	4214	3470	3897	2200
7	T3ms, m/s^2	161	156	134	540 / 589
8	Nij TE	0.959	1.123	0.801	1
9	Nij TF	0.336	0.020	0.020	1
10	Nij CE	0.569	0.486	0.518	1
11	Nij CF	0.255	0.234	0.225	1
12	NIC Rr , m/s^2	77	62	67	-
13	NLow_F, N	1278	1960	1115	2500
14	NUp_F, N	1016	1569	965	2500
15	NLow_M, Nm	75	95	69	-
16	NUp_M, Nm	14	18	13	-

The variation curves for head accelerations are presented in Figure 6 and Figure 7.

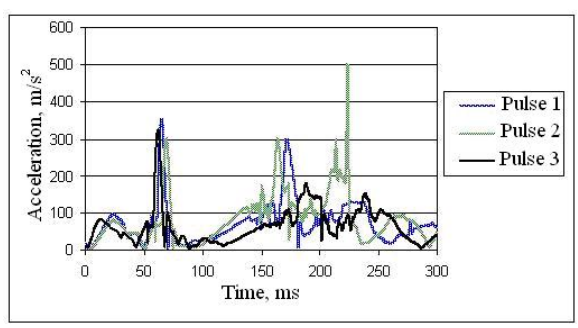

Figure 6. Acceleration pulses, installation with lower anchorages and straps: variation of head linear acceleration.

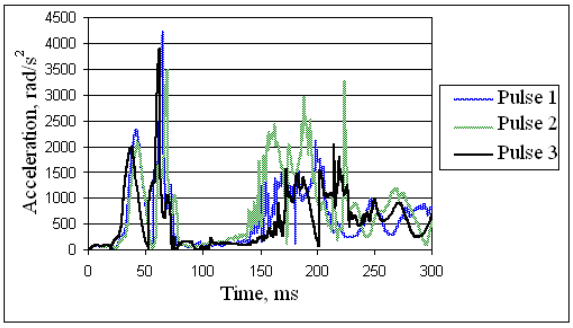

Figure 7. Acceleration pulses, installation with lower anchorages and straps: variation of head angular acceleration.

Figure 8 presents the comparison between the variation curves according to rearward neck injury criteria.

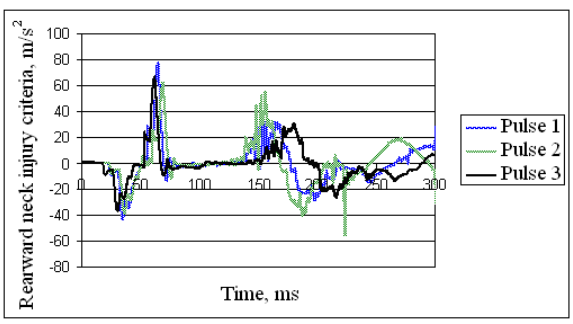

Figure 8. Acceleration pulses, installation with lower anchorages and straps: variation of rearward neck injury criteria.

These comparisons are showing similar variations, except during the last part of the simulations. For head accelerations, two peaks can be observed: the first maximum is toward 60 ms and the second maximum around 220 ms, when the acceleration pulse no. 2 gives the peak for the linear acceleration of the head. The first maximum corresponds to the impact between dummy's head and the child seat back. The second maximum occurred when the head had the greatest displacement and started the backward movement. Its duration is very limited and it was not produced by contact. Consequently, it does not give a significant increase of the HIC.

Comparisons between Installation Configurations

This section presents the simulations' results of the child restraint system when installed using the lower anchors and straps compared to using the vehicle's safety belts. For both installations, the upper part of the child seat back is attached to the vehicle body with a top tether and the child is attached with the harness of the child restraint system. Table 3 presents the comparison between different parameters for the two considered installation configurations, when the rear impact is simulated by the acceleration pulse no. 2 (ΔV=25 km/h, triangular).

Table 3.
Injury criteria comparison for different installation configurations (pulse no. 2)

N°	Parameter	Installation		Ref. value
		Lower anchorages	Safety belts	
1	HIC 15	44	141	570
2	HIC 36	48	154	1000
3	HIC	84	180	1000
4	DT, mm	26	37	34
5	HCG_acc, , m/s^2	501	717	785
6	Hang_acc, rad/s^2	3470	4980	2200
7	T3ms, , m/s^2	156	354	540 / 589
8	Nij TE	1,123	2,229	1
9	Nij TF	0,020	0,746	1
10	Nij CE	0,486	0,444	1
11	Nij CF	0,234	0,272	1
12	NIC Rr , m/s^2	62	249	-
13	NLow_F, N	1960	2792	2500
14	NUp_F, N	1569	2798	2500
15	NLow_M, Nm	95	155	-
16	NUp_M, Nm	18	28	-

Similar simulations have been performed for the other two acceleration pulses.
The variation curves for head accelerations are presented in Figure 9 and Figure 10.

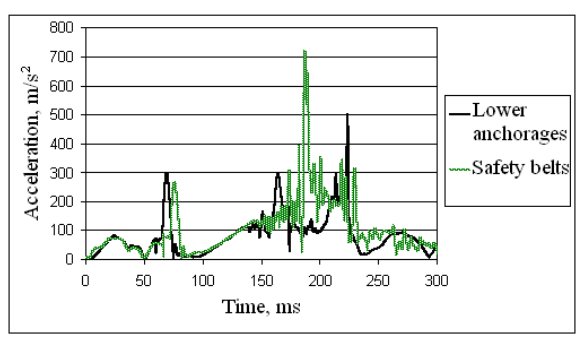

Figure 9. Installations, acceleration pulse no. 2: variation of head linear acceleration.

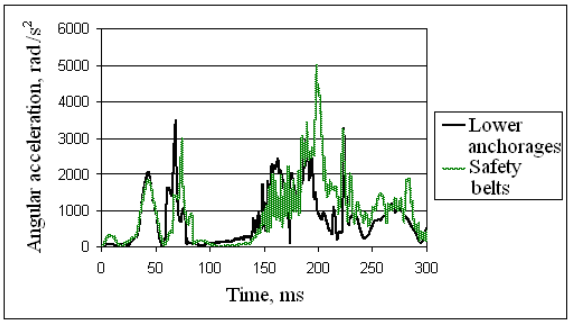

Figure 10. Installations, acceleration pulse no. 2: variation of head angular acceleration.

Figure 11 presents the comparison between the variation curves according to the rearward neck injury criteria.

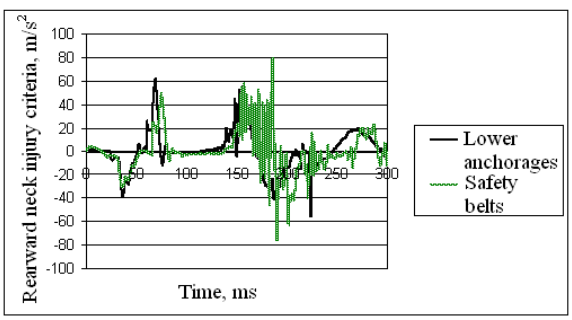

Figure 11. Installations, acceleration pulse no. 2: variation of rearward neck injury criteria.

Table 3 yields also that the admissible values are exceeded only for the neck injury criteria in tension – extension (Nij TE), and this with more than 220 %. For all the parameters, the results for the vehicle safety belt installation are greater than the corresponding results obtained for lower anchorages and straps.
The comparisons of plots shows similar trends but some differences are observed. The curves corresponding to the vehicle safety belts installation are showing more amplitude than the curves obtained with lower anchorages and straps installation. The maximal values in the last part of the simulation are higher for the vehicle safety belt installation, when the head of the dummy reached its maximum displacement and started the backward movement. The linkage is less stiffer and the safety belt segments generate elastic forces producing additional acceleration during the backward movement.
The results show that lower anchorages and straps provide the best protection for the child passenger.

Discussion

This project aimed at the development of a numerical method, using multi-body and finite elements methods, to simulate the behaviour of a child passenger restrained in a protective device while involved in a vehicle rear impact. Simulations have been performed in order to compare the influence of installation configurations and to evaluate the effects of different acceleration pulses.
One of the general limitations of the model is the utilisation of MADYMO belt segments for modelling vehicle safety belts and child seat harness. This type of modelling duplicates very well the geometry of the safety belts and the geometry of the harness, and correctly represents the unidirectional sliding of the belt on dummy's body. Despite these advantages, MADYMO belt segments have fixed attachment points and consequently they do not accurately reproduce the multi-directional sliding
Another category of objective limitations refers to the injury criteria that are not yet well defined and for which does not exist a consensus in the case of a rear impact. We had to use the same criteria normally employed for frontal impact, and available in MADYMO as output data. There are not enough accidentology studies and experimental data are practically inexistent for child passengers involved in a rear impact. Thus, validation of the model for rear impact or, at least, comparing the results of the simulations with test results was not possible. Moreover, there is not yet a child dummy specially destined for the study of rear impact. The Hybrid III dummy was designed for the study of frontal impact and therefore the evaluation of the risk in the case of a rear impact might be also questionable. There are studies showing that the neck of the Hybrid III dummy reproduces well the human response in bending and extension, thus these dummies can be considered for rear as well as for frontal collision evaluations.
A similar situation is met when choosing the acceleration pulses, which are not yet standardized. We used three different acceleration pulses: one acceleration pulse with ΔV = 16 km/h to reproduce low severity accidents, and two acceleration pulses with ΔV = 25 km/h to simulate impacts with more severe consequences.
The comparisons of the simulations results obtained with the three different acceleration pulses show that the acceleration pulse no. 2 (ΔV=25 km/h, triangular) generally gives higher values for the injury criteria than the two other pulses. The result for the neck injury criteria in tension – extension (Nij TE) is the only one exceeding the admissible value, with 12 %. The variation curves for head accelerations are

showing similar variations, excepting the last part of the simulations. For head accelerations, two maximum can be observed: the first is toward 60 ms and the second around 220 ms, when the acceleration pulse no. 2, triangular, with a more abrupt variation of the speed and with the highest amplitude, gives the peak for the linear acceleration for the centre of gravity of the head. The first maximum corresponds to the impact between dummy's head and the child seat back. The second maximum, which has a short duration and not produced by contact, occurred when the head had the greatest displacement and started the backward movement, and it did not significantly increase the HIC.

The comparison of the installation configurations, lower anchorages with straps and vehicle's safety belts, shows that the admissible values are exceeded only for the neck injury criteria in tension – extension (Nij TE). For all the parameters, the results for lower anchorages and straps are less than the corresponding results obtained when the vehicle safety belts were used.

The comparisons of plots shows similar trends but some differences are present. The curves corresponding to the vehicle safety belts installation are showing more variation than the curves obtained with lower anchorages and straps installation. The maximal values in the last part of the simulation are greater for the vehicle safety belt installation, when the head of the dummy reached its maximum displacement before starting the backward movement. The explanation resides in the increased mobility of the installation. Furthermore, the generation of the elastic forces in safety belt segments produce additional acceleration during the backward movement. These considerations entitle preference of the lower anchorages for a better protection of the child passenger.

CONCLUSIONS

The simulations performed with the three acceleration pulses have shown that the neck is the most exposed part of the body. This result is confirmed by the actual preoccupations in the design of the whiplash protection systems. The injury criteria exceed the limit value in certain situations, as in the case of the neck injury criteria in tension-extension with the child restraint system installed using vehicle's safety belts. The result probed is more than double of the limit value.

The acceleration pulse is very important for the accuracy and the realism of the simulations. The simulations were performed under two triangular pulses, with speed variation of 16 km/h and 25 km/h, and one trapezoidal pulse, with speed variation of 25 km/h. In all cases, the results are proportional with the speed variation. Furthermore, the two triangular pulses, with speed variation of 16 km/h and 25 km/h, give higher values for injury criteria than the trapezoidal pulse with speed variation of 25 km/h. The triangular pulse with speed variation of 25 km/h is the most appropriate for a conservative approach.

The comparison of the installation configurations showed that the installation using vehicle's safety belts allows a bigger displacement of the child seat and, consequently of the child dummy.

The rebound caused by the elastic forces is more important, which generates supplementary loads in the neck. Finally, the installation using rigid anchorages and lower straps offers the best protection for the child passenger in the case of rear-end collision.

REFERENCES

Adalian, C., Sferco, R., Fay, P. 2005. "Procedures and Injury Criteria for assessing Neck Injuries in Rear impact." Paper Number 05-0340, 19th International Technical Conference on the Enhanced Safety of Vehicles, Washington, DC.

Boyd, R., Massey, R., Duane, L., Yates, D.W. 2002. "Whiplash Associated disorder in children attending the emergency department." Emergency Medicine Journal, Vol. 19, 311–313.

Croft, A. 2000. "The Risk of Injury for Children Exposed to Whiplash Trauma." Dynamic Chiropractic, Volume 18, Issue 26.

European Vehicle Passive Safety Network 2. 2004. "State-of-the-art Review – Real World Accident and Injury Data." Report: Task 4.1.

Freeman, M., Croft, A., Rossignol, A. 1998. "Whiplash Associated Disorders: Redefining Whiplash and Its Management by the Quebec Task Force: A Critical Evaluation." Spine, Vol. 23(9), 1043-1049.

Hynd, D., van Ratingen, M. 2005. "Challenges in the Development of a Regulatory Test Procedure for Neck Protection in Rear Impacts: Status of the EEVC WG20 and WG12 Joint Activity." Paper Number 05-0048, 19th International Technical Conference on the Enhanced Safety of Vehicles, Washington, DC.

Heitplatz, F., Sferco, R., Fay, P., Reim, J., Kim, A., Pryia, P. 2003. "An Evaluation of Existing and Proposed Injury Criteria with Various Dummies to Determine Their Ability to Predict the Levels of Soft

Tissue Neck Injury Seen in Rear World Accidents." Paper Number 504, 18th International Technical Conference on the Enhanced Safety of Vehicles, Nagoya, Japan.

Kuppa, S., Saunders, J., Stammen, J. 2005. "Kinematically Based Whiplash Injury Criterion." Paper Number 05-021, 19th International Technical Conference on the Enhanced Safety of Vehicles, Washington, DC.

Klinich, K.-D., Sau,l R.-A., Auguste, G., Backaitis, S., Kleinberger, M. 1996. "Techniques for Developing Child Dummy Protection Reference Values." Child Injury Protection Team, NHTSA, U.S. Department Of Transportation.

NHATSA.2002. "Advanced Notice of Proposed Rulemaking (ANPRM) To Add A Side Impact Test to FMVSS No. 213." Preliminary Economic Assessment, Office of Regulatory Analysis and Evaluation Plans and Policy.

NHTSA. 2004. "Child Restraint Systems. Transportation Recall Enhancement, Accountability, and Documentation Act." Report to Congress, U.S. Department Of Transportation.

Sawada, M., Hasegawa, J. 2005. "Development of a New Whiplash Prevention Seat." Paper Number 05-0288, 19th International Technical Conference on the Enhanced Safety of Vehicles, Washington, DC.

Schmitt, K.-U., Muser, M.-H., Niederer, P. 2001. "A Neck Injury Criterion Candidate for Rear-end Collisions Taking into Account Shear Forces and Bending Moments." Paper No. 124, 17th International Technical Conference on the Enhanced Safety of Vehicles, Amsterdam, Netherlands.

Spitzer, W.O., Skovron, M.L., Salmi, L.R., Cassidy, J.D., Duranceau, J., Suissa, S., Zeiss, E. 1995. "Scientific monograph of the Quebec Task Force on Whiplash-Associated Disorders: redefining "whiplash" and its management.", Spine, Vol. 20(8S): 1S-73S.

Surcel, M.-D. 2004. "Simulation du comportement de l'enfant assis dans un dispositif de retenue en cas de collision latérale du véhicule." Master Thesis, École polytechnique de Montréal, ISBN 0494039191.

Surcel, M.-D., Gou, M. 2005. "Development of a mathematical model for evaluating child occupant behaviour in the case of a vehicle side impact simulation. " International journal of Crashworthiness, Vol. 10, No. 1, 111–118.

Transport Canada. 2001. "Test Method 213 — Child Restraint Systems." Standards and Regulations Division.

Versteegen, G.J., van Es, F.D., Kingma, J., Meijler, W.J., ten Duis, H.J. 2001. "Applying the Quebec Task Force criteria as a frame of reference for studies of whiplash injuries." Injury, Volume 32, Issue 3, 185-193.

INFLUENCE OF SEATBACK CONTENT AND DEFLECTION ON FMVSS 202A DYNAMIC RESPONSE

Gerald Locke
Eric Veine
Lear Corporation
Andrew Merkle
Michael Kleinberger
Ian Wing
Johns Hopkins University Applied Physics Laboratory
United States of America
Paper Number 09-0324

ABSTRACT

Automotive seat design requires knowledge of the structural response of the seat under various impact conditions as well as understanding the complex interactions between an occupant, seat content and restraint systems. For the case of rear impact collisions, the seat becomes the primary restraint while seatback and head restraint design become increasingly important in mitigating the risk of occupant injury. This study involved the testing of three different seatback designs under FMVSS 202a dynamic conditions to determine the effects of seatback comfort content on occupant response and injury risk measures. Controlled variables include seatback content and seatback stiffness. Three different recliner stiffness values were simulated that resulted in nominal seatback rotation angles of 5, 10 and 15 degrees. Additionally, three different lumbar support mechanisms were tested, including a static suspension, horizontal lumbar support and vertical lumbar support. Results from the 18 tests conducted are presented and analyzed.

It is expected that the various comfort content will affect torso penetration into the seatback, altering the torso angle and therefore influence the resulting head with respect to torso angle. It is determined that seatback rotation (stiffness) and backset are predictors of head angle and that lumbar support type and foam stiffness affect the backset. The time of maximum head with respect to torso angle (determined as the critical event time) is influenced by seatback stiffness, lumbar support type and lower torso rebound. Both seatback stiffness and lumbar type are found to be good predictors of torso penetration. The amount of torso penetration and the rebound effect on torso angle at the critical time in the event are key findings. None of the independent factors are found to have a significant influence on HIC.

INTRODUCTION

Although injuries associated with low speed rear impacts are typically minor, the annual societal cost associated with these injuries in the US has been estimated at approximately $2.7 billion by the National Highway Traffic Safety Administration (NHTSA) [1]. Based on epidemiological data and scientific research, the NHTSA published the upgraded FMVSS 202a head restraint standard in 2006 [1], which provides a dynamic option for the evaluation of vehicle seats that might perform better in rear impact collisions than their geometric measures may indicate.

Numerous scientific studies have reported connection between neck injury risk and seat design parameters during a rear impact [2-9]. Farmer *et al.* [3] found that active head restraints which moved higher and closer to the occupant's head during rear-end collisions reduced injury claim rates by 14-26 percent. Voo *et al.* [8] evaluated original equipment manufacturer (OEM) seats with active head restraints under dynamic test conditions to determine whether dynamic seat performance correlated with static geometric positioning. Results showed that seat design factors influenced the dynamic performance of the seats.

This study investigates the effects of changes in comfort content and frame stiffness (related to seat adjuster type) under the dynamic option specifications of FMVSS 202a. For seat design, it is important to recognize the difference between frame stiffness and lumbar support system stiffness and their influence on torso penetration into the frame. Relative stiffness of these components affect the amount and timing of torso penetration into the seat, which in turn affect the motion of both the torso and head.

Head displacement relative to the torso during the dynamic event is a function of head support relative to torso support after compression of the foam

covering the structures in these areas. The type of lumbar support or suspension system will affect the dynamic torso angle due to localized stiffness or ability to flex. The type of lumbar support can also affect the H-point location and backset during the initial dummy positioning. The manufacturing variations of seatback and cushion foam properties are known to affect the H-point location, torso angle and backset. H-point height is also directly related to the height of the head restraint. The seat frames, head restraints, foam and trim used in this experiment were of the same design, but with varied torso support features.

METHODOLOGY

Deceleration Sled System

The rear impact vehicle collision environment was simulated with a Via Systems HITS Deceleration sled. The system contains a tunable hydraulic decelerator that absorbs the kinetic energy from the sled carriage and payload by forcing fluid through a series of orifices. The selected orifice array determines the crash pulse experienced by the sled system.

Impact conditions - Rear impact collisions were simulated with a deceleration tuned to the FMVSS 202a Dynamic test pulse.

Adjustable Seatback Stiffness

The standard dual recliners that connect the seat cushion frame to the seatback frame were modified so that they became free-pivots. Each seatback was modified to accommodate a C-channel frame for interfacing with a spring-damper assembly (Figure 1) used to control seatback rotational stiffness.

The frame allowed for variable positioning of the support system and modifications of seatback rotational stiffness. Spring stiffness and position settings for targeted seatback rotations of 5, 10 and 15 degrees were selected using predictive models. The settings for the test conditions are provided in Table 1.

Table 1.
Simulated recliner stiffness for desired magnitudes of rotation

Nominal Rotation (degrees)	Recliner Stiffness (Nm/degree)
5	219
10	108
15	71

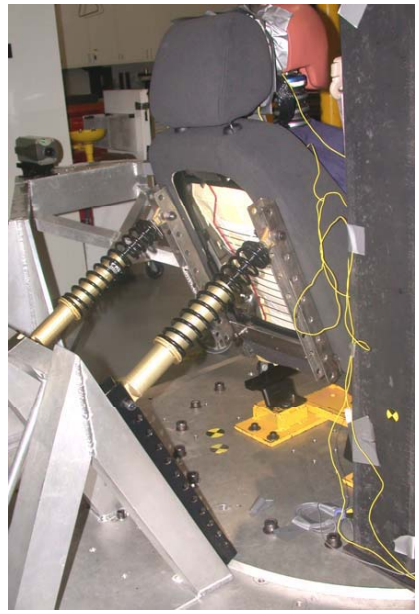

Figure 1. Seat system and spring-damper assembly.

Instrumentation and Data Acquisition

The coordinate system used for the Hybrid III and sled is shown in Figure 2. The dummy was instrumented with tri-axial accelerometer arrays at the center of gravity (CG) of the head, torso and pelvis. Six-axis load cells, sensing tri-axial forces and moments, were installed in the upper and lower neck and a three-axis load cell was placed in the lumbar spine.

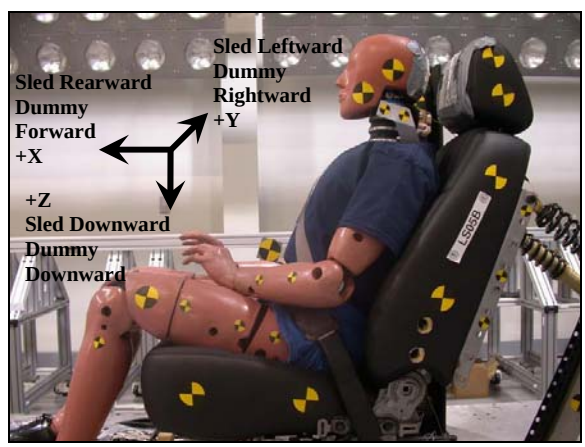

Figure 2. Sled and Hybrid III coordinate system.

Angular rate sensors were attached at the head CG and the spine at T4. An accelerometer was mounted to the sled to record the deceleration during impact. The complete list of the instrumentation used during

these tests is provided in Table 2. All designated polarities, filtering, and sampling rates were determined in accordance with SAE Recommended Practice J211. All sensor data were collected at a sampling rate of 10 kHz using an on-board TDAS Pro data acquisition system mounted to the sled base plate.

Table 2.
Sled and ATD instrumentation

Sensor	Location
Accelerometer	Sled (x)
Head Contact Switch	Head-Head Restraint
Angular Rate Sensor	Head (y)
Angular Rate Sensor	Torso (y)
Accelerometer	Head CG (x,y,z)
Accelerometer	Torso CG (x,y,z)
Load Cell	Upper Neck (Fx,Fy,Fz,Mx,My,Mz)
Load Cell	Lower Neck (Fx,Fy,Fz,Mx,My,Mz)
Load Cell	Lumbar (Fx,Fz,My)
Accelerometer	Pelvis (x,y,z)

High-speed Video

Video images were captured at 1000 frames per second with one on-board and one off-board camera. The on-board camera, used for motion analysis, has a resolution of 512x512 and was mounted to provide a left lateral view of the dummy kinematics from a fixed distance of approximately 5 feet. Video collection was synchronized with the data acquisition system using both a contact switch and optical flash within the field of view. Examples of the captured images during impact are provided in Figure 3.

Figure 3. High-speed camera views at 111 milliseconds for test LH15C.

Quadrant targets were attached to the ATD to allow for motion tracking including the calculation of angular displacement measurements and the amount of torso displacement. Key targets were attached to the upper spine box and lower spine box to determine torso movement. Torso penetration is defined as the amount the torso translated toward the seatback frame with respect to the normal of the C-channel located on the seatback frame. Targets were also placed on the seat system, the C-channel and the supporting A-frame.

Experimental Protocol

<u>ATD Positioning Procedure</u> - Proper installation of the Hybrid III into the seat system required a multi-step process. First, the seat system was installed on the sled baseplate and the seat cushion and adjuster assembly was adjusted to the mid-point of the track. A spring-damper support system was then installed to support the seatback. The lengths of the supports were adjusted to maintain a nominal SAE J826 H-point machine torso angle of 25 degrees with respect to the vertical plane when the seat is in static equilibrium with the H-point machine seated. FMVSS 202a specifies that the seatback angle, as determined by the torso angle of the installed H-point machine, must reside between 24.5 and 25.5 degrees. If this specification was met, we continued the positioning procedure, if not, the H-point machine was removed completely and the positioning procedure was repeated.

Upon satisfying the angle specifications, the seat H-point location was measured. Next, the Head Restraint Measuring Device (HRMD) was installed to measure backset and head-to-head restraint height when it was set to the locking notch just lower than mid-height (if there is no locking notch at mid-height), according to the specifications of FMVSS 202a.

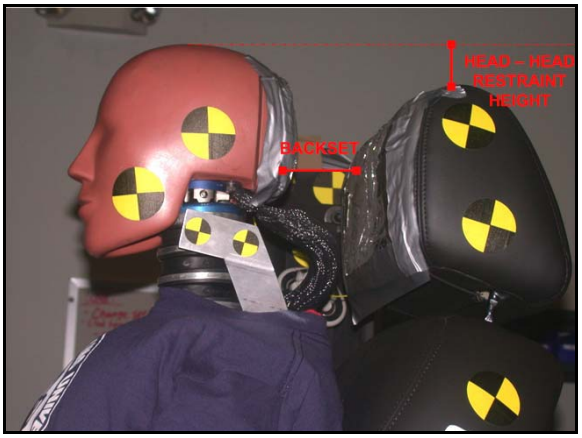

Figure 4. Measurement of Hybrid III backset and head-to-head restraint height.

The H-point machine and HRMD were then removed and the 50% Hybrid III dummy was placed on the seat and positioned such that the head was level and the dummy H-point was within 0.5 inches of the measured seat H-point location. Initial dummy head positioning included a measure of the head angle with respect to horizontal, the effective backset and the height difference between the top of the head and the head restraint (Figure 4). The horizontal (X) and vertical (Z) H-point location of the dummy relative to the measured seat H-point was recorded.

Test Matrix - Three seat systems were being studied (Table 3) with the difference between systems determined by the seat content in the form of lumbar support. The three seatback content types were categorized as vertical lumbar, horizontal lumbar and static suspension systems (Figure 5). Three nominal levels of rotation (5, 10, and 15 degrees) were selected for study. This results in a total of nine test combinations. Conducting a full factorial experimental design and replicating it once produced a test matrix consisting of 18 impact tests.

Table 3.
Independent factors contributing to the design of the test matrix

Factor	No.	Categories
Seatback Content	3	Static Suspension, Horizontal Lumbar, Vertical Lumbar
Seatback Rotation (deg)	3	5, 10, 15

Figure 5. Seatback content types.

The picture (Figure 5) shows the structural differences between the three lumbar support systems which include a) static suspension, b) horizontal and c) vertical lumbar support systems from left to right. The static suspension is a wire mesh supported by vertical wires attached at the upper and lower frame cross-members and two springs, one attached one-third of the distance up from the bottom of each side-member. The horizontal lumbar is a plastic strap supported by flexible brackets attached to each frame side-member and a cable fixed to each bracket. The vertical lumbar is a sheet metal panel supported by vertical wires attached at the upper and lower frame cross-members. Some of the adjustment mechanism is between the panel and the frame lower cross-member. All adjustable lumbar supports are set to the fully retracted position for the FMVSS 202a Dynamic procedure.

RESULTS AND DISCUSSION

Test Sample Measurements

Tables 4 and 5 list the H-point location and head restraint backset and height dimensions for both the H-point machine/HRMD and Hybrid III by lumbar support type.

Initial frame angle - One of the main issues with foam and trim variation, as well as differences in the way a lumbar type supports the seatback foam, is that this may require the seatback frame angle to be varied in order to achieve the H-point machine torso angle of 25 degrees. In Table 5 we can see that this is not a problem for these tests as the initial seatback frame angle was controlled reasonably well and varied by a maximum 1.6 degrees for the horizontal lumbar and 1.1 degrees for the static suspension and the vertical lumbar. The Hybrid III is then positioned by the FMVSS 208 procedure without adjusting the frame angle.

Table 4.
SAE J826 and Hybrid III H-point coordinates and SAE J826/HRMD backset and height

Test ID	Seat Content	J826 H-pt		HIII H-pt		HRMD	
		x	z	x	z	Backset	Height
		(mm)	(mm)	(mm)	(mm)	(mm)	(mm)
LH05A	Horz.	11	-26	20	-21	63	65
LH05B	Horz.	16	-26	17	-31	65	65
LH10B	Horz.	13	-17	16	-21	63	66
LH10C	Horz.	22	-24	29	-26	69	67
LH15B	Horz.	23	-26	22	-26	63	65
LH15C	Horz.	22	-23	27	-22	68	72
LS05A	Static	8	-14	8	-20	84	69
LS05B	Static	9	-18	8	-23	77	75
LS10B	Static	7	-25	9	-27	80	74
LS10C	Static	17	-25	19	-24	63	69
LS15B	Static	7	-29	8	-33	77	69
LS15C	Static	16	-25	21	-25	84	69
LV05C	Vert.	16	-24	16	-24	76	62
LV05E	Vert.	20	-23	22	-28	73	69
LV10A	Vert.	13	-29	14	-28	79	71
LV10B	Vert.	16	-24	18	-22	80	70
LV15A	Vert.	11	-17	9	-18	72	67
LV15B	Vert.	10	-25	11	-31	75	71
H-pt coordinates are with respect to the design H-point reference.							

Table 5.
Initial seatback frame angle, Hybrid III backset and height, actual maximum seatback rotation angle and head restraint contact time

Test ID	Seat Content	Initial Frame Angle (degrees)	HIII H/R Backset (mm)	HIII H/R Height (mm)	Max. S/B Rotation (degrees)	H/R Contact Time (msec)
LH05A	Horz.	21.9	71	52	7.5	60
LH05B	Horz.	22.7	84	51	7.7	65
LH10B	Horz.	22.4	87	55	10.5	69
LH10C	Horz.	23.5	85	53	10.5	68
LH15B	Horz.	21.9	84	50	14.4	73
LH15C	Horz.	22.7	77	58	13.3	76
LS05A	Static	23.0	108	53	7.4	72
LS05B	Static	22.7	104	61	7.2	70
LS10B	Static	23.1	108	60	10.6	74
LS10C	Static	22.3	88	63	10.7	65
LS15B	Static	22.3	101	55	13.9	76
LS15C	Static	23.4	105	52	14.0	74
LV05C	Vert.	22.9	95	52	7.8	68
LV05E	Vert.	22.5	104	57	7.7	68
LV10A	Vert.	22.9	99	57	10.4	69
LV10B	Vert.	23.6	111	63	10.4	77
LV15A	Vert.	22.6	96	55	14.3	75
LV15B	Vert.	22.5	94	60	13.6	73

Backset - The backset and height of these seats were not varied by experimental design. The differences are caused by a combination of foam properties, lumbar support type and initial seatback frame angle. The mean backsets in Table 6 are calculated by lumbar support type. Lumbar type appears to be the dominant factor for influencing backset where the horizontal lumbar and static suspension have the smallest and largest backsets, respectively.

Table 6.
Backset mean by lumbar support type

Lumbar Support Type	Backset mean (mm)
Horizontal Lumbar	81
Static Suspension	102 (105 without LS10C)
Vertical Lumbar	100

Referring to Tables 4 and 5, one particular seat backset, LS10C, stands out as being well below the mean of the other five static suspension seats. It is of the same design, but the seatback foam was manufactured at a later date. This is an example of the manufacturing difficulties of controlling foam properties. This foam is easier to compress with the H-point machine and Hybrid III upper torso. The upper torso (shoulders) and lower torso (top of lumbar sine) are approximately 20 mm and 10 mm closer to the seatback frame than LS10B, respectively, as judged by the backset and H-point data. This will also be seen in the torso penetration data later in the discussion.

Head contact time - The head contact time with the head restraint in Table 5 was found to depend upon backset and frame stiffness. The head restraint contact time increases as frame stiffness decreases for all lumbar types. For greater frame stiffness, the contact time increases with a backset increase. The difference in head contact time relative to backset appears to diminish as the frame stiffness decreases.

The Hybrid III head restraint height, referenced down from the top of the head, differs by a maximum 13 millimeters for all tests. This difference is caused by seat cushion foam property and head restraint dimensional variations. It will influence the results if the head center-of-gravity becomes higher than the top of the head restraint structure due to ramping of the dummy upward with respect to the seatback. Ramping of the dummy may be affected by the stiffness of the lumbar support system and seatback rotation angle which will be discussed.

Acceleration pulse - The acceleration pulses for all tests are shown in Figure 6. The onset of all accelerations and the peak values, with a few exceptions, are within the required corridor. The repeatability is acceptable for this test series, however two pulses, LS05B and LH15C, show a significant early reduction in magnitude before the peak and fall below the corridor. All pulses are slightly long in time duration.

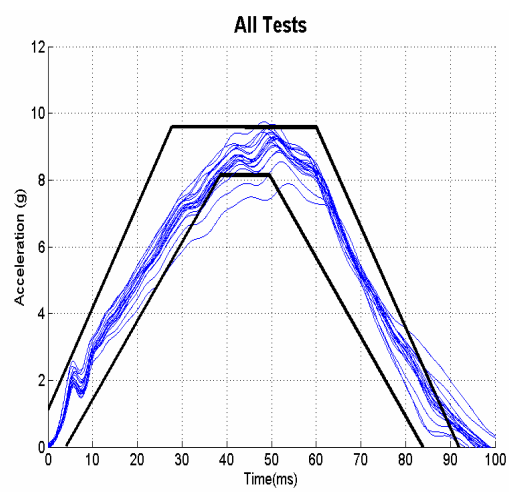

Figure 6. Sled pulses for all tests.

Table 7 lists the impact velocities and the peak deceleration for all tests. The effect of the low pulses will be considered during the discussion. The initial dummy positioning and the backsets for tests LS05B and LH15C were very similar to their respective repeat tests. The torso angles were lower and the head angles were considerably lower, resulting in

reduced head with respect to torso rotation (H-T rotation). This will be discussed in greater detail in the following sections.

Table 7.
Sled acceleration peaks and velocities

Test ID	Impact Vel. (km/h)	Peak Decel. (g)
LH05A	17.3	9.0
LH05B	17.5	9.3
LH10B	17.4	9.2
LH10C	17.8	9.4
LH15B	17.7	9.7
LH15C	16.3	7.9
LS05A	17.2	9.1
LS05B	16.6	8.6
LS10B	17.3	9.3
LS10C	17.7	9.5
LS15B	17.4	9.2
LS15C	17.7	9.4
LV05C	17.4	9.3
LV05E	17.3	8.9
LV10A	17.3	9.4
LV10B	17.3	9.0
LV15A	17.8	9.7
LV15B	17.0	8.8

Seatback rotation - Figure 7 shows that the actual seatback rotation angles are above the 5 and 10 degree targets and below the 15 degree target, but are reasonably repeatable. The largest variation for the same type of test is 1 degree for the horizontal lumbar at 15 degrees of rotation and is likely caused by the low pulse in LH15C. The spacing of these responses clearly delineates three discrete populations for investigating the influence of seatback stiffness.

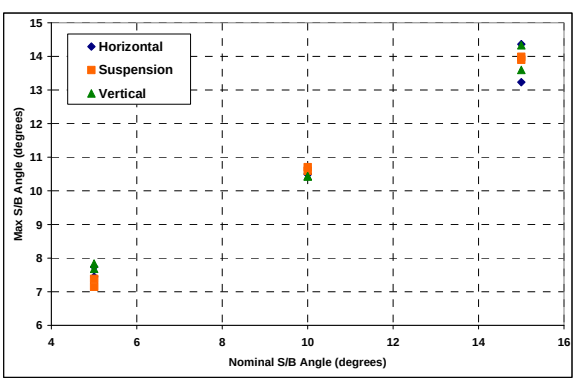

Figure 7. Actual maximum seatback rotation angles.

Note that the data used throughout the balance of this discussion is motion analysis data. Rigidly mounted quadrant targets were used in all cases rather than quadrant targets attached to flexible seat trim. Angular rate sensors were used to derive the head and torso angles and compared to motion analysis results. This comparison can be found in the appendix. The differences are acceptable and motion analysis includes additional data such as seatback rotation, upper and lower torso initial distance from the seatback frame, penetration towards the frame, x- and z-translation and head restraint angular displacement.

Figure 8 is the 15 degree seatback rotation time-history for all lumbar types and shows that the rate of rotation is greater for the horizontal lumbar which is the stiffest lumbar type. The more flexible static suspension and vertical lumbar have the lowest rate. This effect can be seen for all seatback rotation angles, but is less pronounced as the seatback stiffness increases.

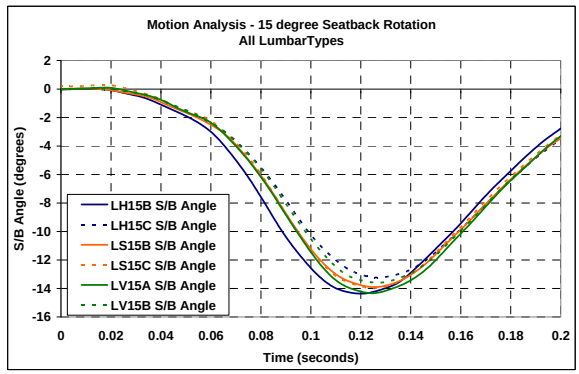

Figure 8. 15 degree seatback rotation for all lumbar types.

Head restraint angular displacement - Figure 9 shows the head restraint angular displacement relative to the seatback frame at the time of maximum H-T rotation. For greater seat stiffness, an increase in head restraint angular displacement relative to the seatback frame is observed. The displacement is lower for the horizontal lumbar and is likely related to the greater seatback rotation rate.

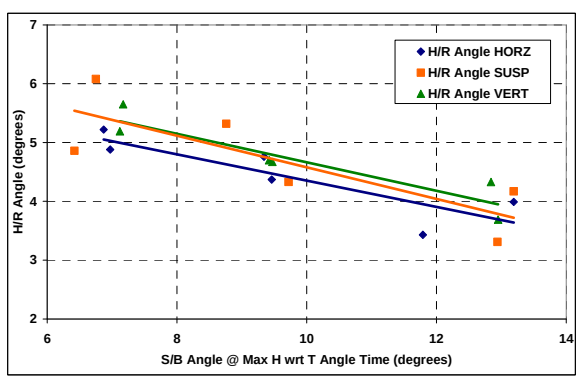

Figure 9. Head restraint angular displacement @ maximum H-T rotation time.

HIC$_{15}$ – The HIC$_{15}$ values in Table 8 are very low compared to the FMVSS 202a limit of 150. The construction of the head restraints consists of a semi-rigid expanded polypropylene core attached to a 10 millimeter diameter solid frame (and posts) covered by 20 mm of polyurethane foam and a trim cover. The stiff head restraint construction used in the experiments had no detrimental effect. Statistical analyses showed that seatback rotation and lumbar support types were not significant in influencing HIC.

Table 8.
HIC$_{15}$ Values

Test ID	HIC$_{15}$
LH05A	36
LH05B	38
LH10B	29
LH10C	34
LH15B	41
LH15C	29
LS05A	40
LS05B	31
LS10B	34
LS10C	29
LS15B	36
LS15C	42
LV05C	31
LV05E	39
LV10A	33
LV10B	38
LV15A	36
LV15B	37

Hybrid III ramping – The z-direction displacement relative to the seatback frame will show the effect of lumbar type and seatback rotation on Hybrid III ramping. The z-axis is parallel to the seatback frame and rotates with the seatback. Increased ramping may reduce the effectiveness of the head restraint, depending on the initial height. Figure 10 shows the upper torso z-direction displacement for all lumbar types at the 15 degree seatback rotation angle.

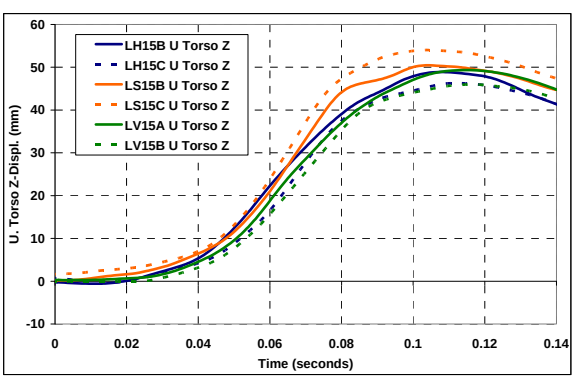

Figure 10. Upper torso z-axis displacement - 15 degree seatback rotation – all lumbar types.

The 15 degree seatback rotation proves to generate the greatest ramping, but only a few millimeters more than other cases. The static suspension is slightly greater in magnitude and peaks slightly earlier. At all seatback rotation angles, all lumbar types allow essentially the same amount of ramping (see appendix).

Hybrid III segment angles - The Hybrid III head and torso rotation time-histories are used to calculate the maximum head with respect to torso rotation (H-T rotation). This angle is the maximum difference between the head and torso rotation at any point in time during the event, up to 200 milliseconds. The time of maximum H-T rotation is studied for the influence of lumbar support type and seatback rotation. Much of the data presented will be at this critical time.

Figure 11 shows that the changes in head rotation at each seatback stiffness level are generally greater than the increase in seatback rotation at the time of maximum H-T rotation. The exception is for the vertical lumbar for which the rate of head rotation increase is approximately equivalent to that of seatback rotation. This implies that head support generally degrades as seatback rotation increases although the head restraint angular displacement findings (Figure 10) show that it has less displacement at greater seatback angles.

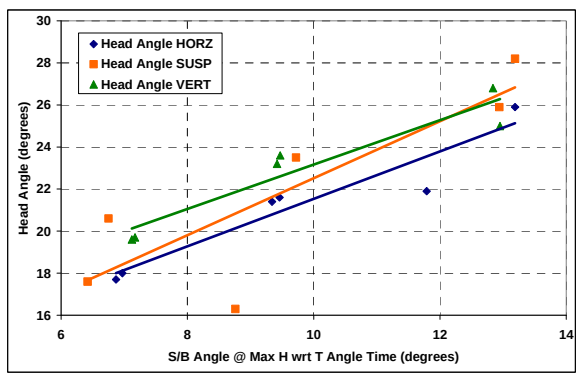

Figure 11. Head angle @ maximum H-T rotation time.

The static suspension shows the largest variation at the ten degree seatback rotation. The lowest head angle is test LS10C seat which has a backset much smaller than the average of the other static suspension seats. The horizontal lumbar consistently has the lowest head angles and it also has the lowest average backset of all lumbar types. However, backset is not the only contributor to head support. The distance of shoulder penetration will also affect

head angle. An analysis of upper torso penetration is conducted in the following sections.

Similar to observations with head rotation, Figure 12 shows that changes in torso angle for each seatback stiffness condition increase at a rate greater than that of seatback rotation at the time of maximum H-T rotation. There does not appear to be a significant influence of lumbar support type on torso angle. The vertical lumbar does exhibit a slightly greater torso angle, particularly at the 10 degree seatback rotation. The distance of the upper and lower torso penetration at critical time as well as the rebound will be analyzed to help understand this as well as the affect on head support.

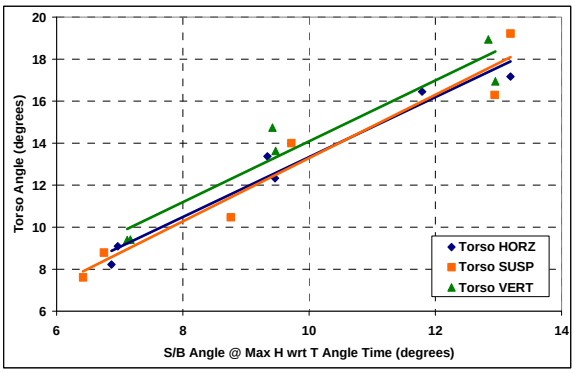

Figure 12. Torso angle @ maximum H-T rotation time.

Figure 13 shows the time-history of the Hybrid III segment angles for the static suspension repeat tests at 10 degree seatback rotation. These tests represent the greatest difference in head angles between repeats due to the LS10C backset (Table 5) as discussed earlier. The maximum head angle occurs just after critical time and just before the time of maximum seatback rotation. The maximum torso angle occurs well after maximum seatback rotation. These observations apply to all tests.

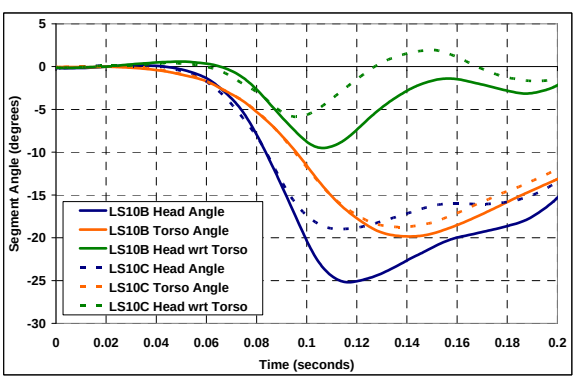

Figure 13. HII segment angles for the static suspension - 10 degree seatback rotation.

<u>Torso Penetration</u> - The starting point of each curve is the initial distance of the torso target to a line on the structure attached to the seatback frame and parallel to the seatback frame. The x-axis is normal to the seatback frame and rotates with the seatback. The magnitude becomes smaller as the torso displaces toward the seatback frame.

Figure 14 shows the upper torso penetration towards the seatback frame of the static suspension tests at all seatback rotation angles. At the critical time, the upper torso has penetrated to its maximum for the 5 and 10 degree seatback rotation angles. While all penetrations are fairly stable at this time, the 15 degree rotation tests have not yet reached their maximum and the 5 degree rotation is in rebound shortly after. This is typical for all lumbar types.

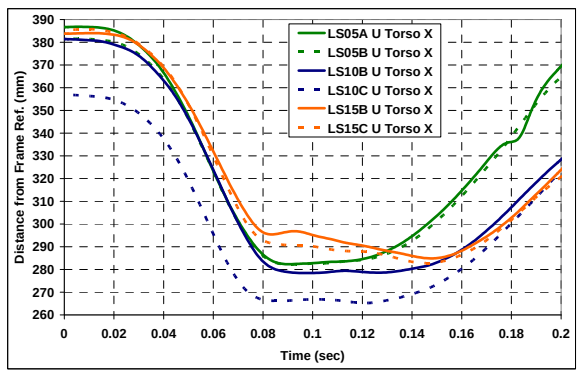

Figure 14. Upper torso x-direction penetration - static suspension - all seatback rotation angles.

The LS10C initial position shows why the backset is smaller for this test. The LS10C upper torso penetration is deeper than LS10B, reinforcing the low foam stiffness observation.

Figure 15 shows the upper torso penetration for all tests at the time of maximum H-T rotation. The upper seatback should present less resistance to the torso as it rotates at the greater angles since more energy is being absorbed by the spring-damper controlling the rotation. The horizontal lumbar is most representative of this theory. However, the static suspension and vertical lumbar both show an increase in penetration for the 10 and 15 degree seatback rotations. This should result in lower head angles (Figure 11), but does not because the head restraint angular displacement (Figure 9) is also greater. The static suspension and vertical lumbar both allow more force to be distributed to the upper seatback due to their inherent flexibility and method of attachment to the frame. This distribution of force along the seatback supports the finding of the lower rate of seatback rotation (Figure 8).

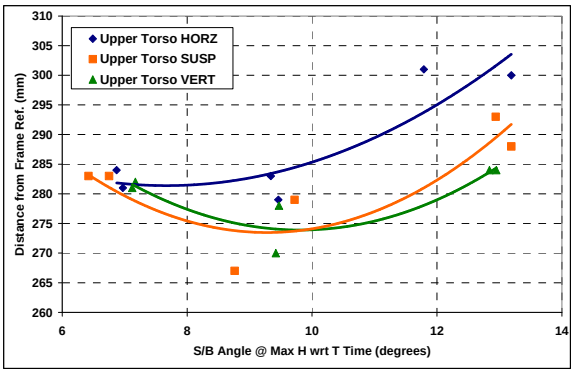

Figure 15. Upper torso penetration @ maximum H-T rotation time.

Figure 16 shows that the lower torso is in rebound at the time of maximum H-T rotation for the static suspension tests at all seatback rotation angles. This is typical for all lumbar types.

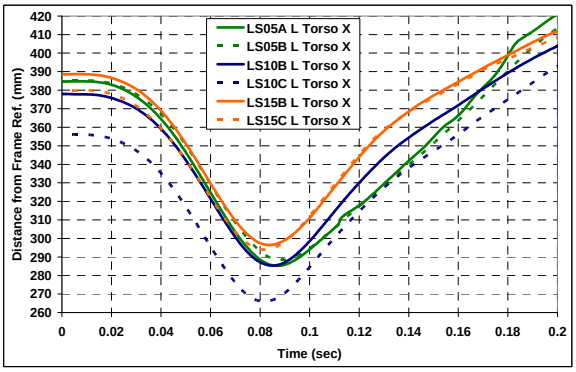

Figure 16. Lower torso x-direction penetration - static suspension - all seatback rotation angles.

It is a key finding that the torso angle is increasing at relative to the seatback frame at the time of maximum H-T rotation. Since the upper torso remains at a stable or increasing penetration, this lower torso rebound is a major factor of torso angle and is likely susceptible to changes in the stiffness and energy return of a lumbar support system. If the lower torso rebound occurs earlier or is larger in magnitude, the head with respect to torso angle will be reduced.

Both torso penetration plots (Figures 14 and 16) also show the initial distance of the torso targets to the seatback frame reference line. These targets are at the same locations on the dummy and the seatback for all tests. This data shows the variation in dummy set-up due to what is believed to be foam variation, not mechanical or dimensional differences in the static suspensions. Foam stiffness is known to vary with temperature and humidity differences during the manufacturing process. The torso penetration plots for the horizontal and vertical lumbar supports are available in the appendix for review.

The lower torso x- and z-axis displacement at the 10 degree seatback rotation in Figure 17 shows some differences in displacement characteristics of lumbar types. The horizontal lumbar is able to restrain the Hybrid III pelvis/lumbar while the static suspension and vertical lumbar provide restraint to a lower extent. This explains why the static suspension and vertical lumbar upper torso continues to penetrate. This data is truncated at the time of maximum H-T rotation.

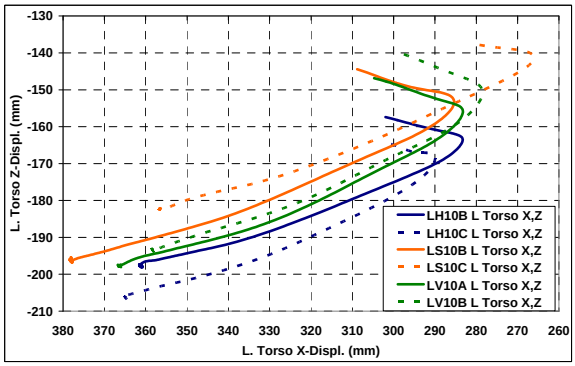

Figure 17. Lower torso x- & z-axis displacement @ 10 degree seatback rotation – all lumbar types.

The maximum lower torso penetration for all tests in Figure 18 shows that the horizontal lumbar has the highest resistance to penetration at all seatback rotations. The static suspension is the least resistant to torso penetration with the exception of the 15 degree seatback rotation where it is the same as the vertical lumbar. The seatback frame lower cross-member is contacted in all tests as evidenced by permanent deformation that increases in magnitude with seatback stiffness. The resistance to lower torso penetration by the horizontal lumbar shows that it transfers more force to the lower portion of the seatback frame which increases the rate of seatback rotation (Figure 8).

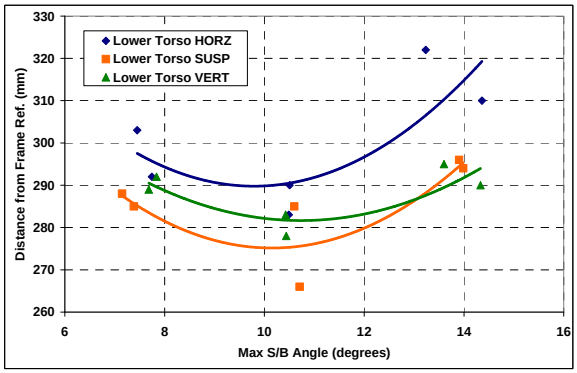

Figure 18. Maximum lower torso penetration.

The lower torso rebound from maximum penetration at the time of maximum H-T rotation in Figure 19 shows that rebound increases as the seatback rotation increases. There is little difference in the magnitude of all lumbar types. The amount of rebound appears to be mainly a function of time. This time is the difference in the time of maximum penetration and the time of maximum H-T rotation. If the time difference increases as the seatback rotation increases, then there is more time for lower torso rebound and this will result in an increase of the torso angle.

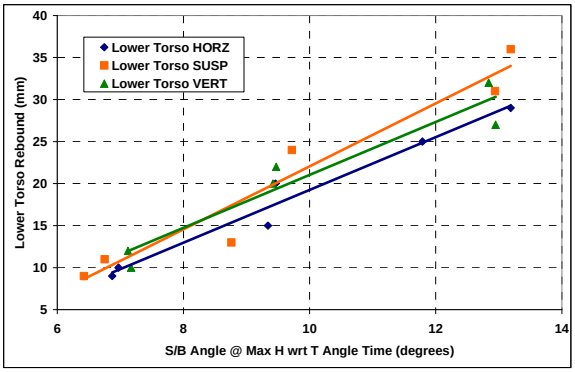

Figure 19. Lower torso rebound @ maximum H-T rotation time.

Since the horizontal lumbar has no energy storage and return properties and the lower torso still exhibits substantial rebound, rebound must be a mainly a function of time rather than the mechanical properties of the lumbar type. Table 9 lists the time duration of the rebound from maximum lower torso penetration to the time of maximum H-T rotation.

Table 9.
Time duration of lower torso rebound

Test ID	Max. Penetration Time (msec)	Max H-T Rotation Time (msec)	Rebound Duration (msec)
LH05A	83	98	15
LH05B	83	98	15
LH10B	82	103	21
LH10C	80	100	20
LH15B	79	104	25
LH15C	84	109	25
LS05A	87	102	15
LS05B	87	103	16
LS10B	85	107	22
LS10C	82	97	15
LS15B	84	110	26
LS15C	82	111	29
LV05C	86	100	14
LV05E	85	102	17
LV10A	82	103	21
LV10B	85	105	20
LV15A	83	107	24
LV15B	84	112	28

The lower torso penetration peaks earliest at the 5 degree seatback rotation for the horizontal lumbar, otherwise all results are similar. The time of maximum H-T rotation is delayed as seatback stiffness decreases, therefore the time duration of lower torso rebound increases as seat rotation increases. The static suspension and the vertical lumbar have a slightly longer rebound time duration at the 15 degree seatback rotation.

For the lower torso penetration at the time of maximum H-T rotation (Figure 20), the horizontal lumbar, with no significant spring characteristics, is farthest from the frame. The static suspension appears to have more energy return due to the spring tension at mid-height of the frame. At the 15 degree seatback rotation, it reduces the distance between it and the horizontal lumbar at maximum penetration. The vertical lumbar, which has long spring-steel wire supports, shows a similar characteristic at the 15 degree seatback rotation.

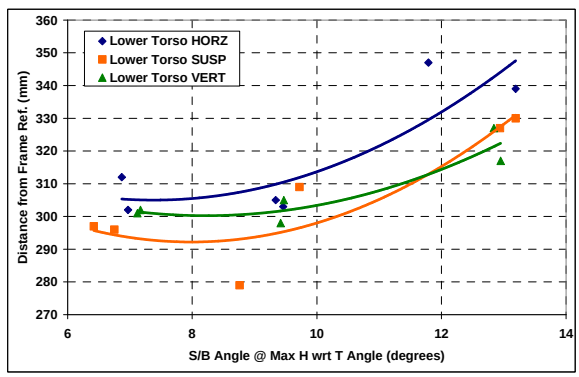

Figure 20. Lower torso penetration @ maximum H-T rotation time.

The maximum H-T rotation in Figure 21 is one of the compliance requirements of FMVSS 202a with a twelve degree maximum. The largest variations occur with the static suspension and the horizontal lumbar at 10 and 15 degree seatback rotations, respectively. The LS10C is the lowest due to the low head angle caused by the smaller backset (Table 5) and low seatback foam stiffness described earlier. The lowest horizontal lumbar point is LH15C and is due to the low head angle caused by the low pulse (Table 7).

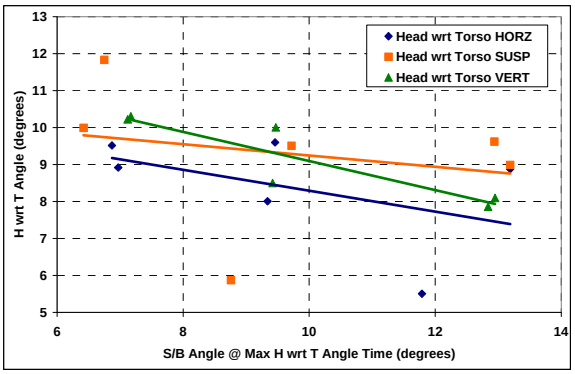

Figure 21. Maximum H-T rotation.

Considering the small differences in torso angles (Figure 12), the static suspension generally has the greatest maximum H-T rotation which is caused by greater head angles (Figure 11). This is mainly attributed to larger backsets caused by the most prominent seatback foam support (Table 6). The vertical lumbar provided seatback foam support similar to the static suspension and has similar backsets. Given the similar head angles and slightly greater torso angles, it performed slightly better than the static suspension. The horizontal lumbar has the lowest head with respect to torso angles because of the lower head angles. This is attributed to approximately 20 millimeter smaller backsets caused by the least prominent seatback foam support which offsets the approximate 10 millimeter reduction in shoulder penetration.

CONCLUSIONS

During test set-up, the backset is affected by both lumbar type and foam stiffness variation. The static suspension provided more prominent support of the seatback foam and tended to increase the backset. The largest foam variation, a reduction in foam stiffness in one static suspension test, caused a significant reduction in backset. During that test event, the torso penetration was also the greatest of all tests. This resulted in the earliest head contact time, the lowest head rotation and the lowest H-T rotation (for a valid pulse). For all other tests with reasonably consistent foam properties, the static suspension tends to have the highest H-T rotation. Therefore, seatback foam properties have a significant influence on head support with more compliant foam improving head support.

The HIC_{15} is low for all tests and did not appear to be affected by the stiff head restraint construction or the controlled parameters of seatback rotation or lumbar support type.

The head restraint angular displacement relative to the seatback frame increases as seatback stiffness increases, however the horizontal lumbar tests have lower head restraint displacement and head angle. The horizontal lumbar provides greater restraint of Hybrid III pelvis/lumbar displacement due to the attachment at the frame side-members and relative inability to flex rearward. The horizontal lumbar increases the rate of seatback rotation, reducing the upper torso penetration, head restraint displacement, head rotation and H-T rotation. Therefore, a stiff lumbar support attached in a manner that limits rearward displacement reduces maximum H-T rotation.

Ramping of the Hybrid III, which may reduce the effectiveness of the head restraint, was not significantly effected by lumbar support type or seatback stiffness.

Head angle increases at a greater rate than the controlled maximum seatback rotations, regardless of the head restraint angular displacement finding. Torso angle also increases at a greater rate than the controlled maximum seatback rotations. This is due to stable upper torso penetration and lower torso rebound at the time of maximum H-T rotation. Lower torso rebound is found to be a mainly a function of time rather than a function of the energy return characteristics of lumbar type. The maximum torso penetration is a function of lumbar support stiffness, foam stiffness and seatback stiffness. The maximum torso penetration and the amount of time for lower torso rebound determine the torso angle at the time of maximum H-T rotation.

In this experiment, the horizontal lumbar proved to have the highest resistance to lower torso penetration. Maximum lower torso penetration time is essentially the same for all lumbar types and seatback stiffness with only a slight delay for the more flexible lumbar support types. The time to maximum H-T rotation increases as the maximum seatback rotation increases. This results in greater lower torso rebound time and distance as the maximum seatback rotation increases. Therefore, there is an increase in torso angle at maximum H-T rotation time as the maximum seatback rotation increases. This results in a lower maximum H-T rotation.

RECOMMENDATIONS

Head support is reduced as seatback rotation increases as evidenced in the head angle discussion. Therefore, decreasing the seatback stiffness (adding to lower torso rebound time) to increase torso angle is

probably neutralized at some undetermined maximum seatback rotation. If comfort specifications allow, it would be recommended to reduce the backset (to reduce head angle) and/or stiffen the lumbar support mechanism to reduce lower torso penetration (to increase torso angle) at the critical time to improve the Hybrid III maximum H-T rotation result.

A follow-up study will be done to analyze the Hybrid III neck forces and moments collected during this experiment.

STUDY LIMITATIONS

Listed are some notable limitations of this study:

- The width of the seatback frame may affect the ability of the torso to penetrate regardless of the lumbar support system.
- The stiffness of the head restraint posts and the attachment to the seatback frame may affect the amount of head restraint angular displacement relative to the seatback.
- The amount and properties of compressible foam covering the seat structure.
- The construction of the head restraint, backset and height.
- The type of anthropomorphic test device (dummy), particularly spine flexibility, may affect the results.

All of these seat design factors vary with seat manufacturer and vehicle model styling requirements. Other rear impact simulation protocols specify different crash pulses and dummy types. The observations reported here are directionally correct for the Hybrid III dummy, but the magnitude will vary with other seat types.

ACKNOWLEDGEMENT

The authors would like to thank Arjun Yetukuri, Liming Voo, Howard Conner and Bethany McGee for their contributions to the planning and execution of this test series.

REFERENCES

[1] NHTSA Final Rule. "Federal Motor Vehicle Safety Standards: Head Restraints." Docket No. NHTSA-2004-19807, RIN 2127-AH09, 2006.

[2] Eichberger A, Geigl BC, Moser A, Fachbach B, Steffan H, Hell W, Langwieder K. "Comparison of Different Car Seats Regarding Head-Neck Kinematics of Volunteers during Rear End Impact," International IRCOBI Conference on the Biomechanics of Impact, Dublin, September, 1996..

[3] Farmer, C., Wells, J., Lund, A., "Effects of Head Restraint and Seat Redesign on Neck Injury Risk in Rear-End Crashes," Report of Insurance Institute for Highway Safety, October, 2002.

[4] Kleinberger M, Voo L, Merkle A, Szczepanowski R, and McGee B. A comparative study of dummy sensitivity to seat design parameters. 20th Enhanced Safety of Vehicles Conference, Paper No. 07-0366, Lyon, France, June, 2007.

[5] Kleinberger M, Voo LM, Merkle A, Bevan M, Chang S, "The Role of Seatback and Head Restraint Design Parameters on Rear Impact Occupant Dynamics," Proc 18th International Technical Conference on the Enhanced Safety of Vehicles, Paper #18ESV-000229, Nagoya, Japan, May 19-22, 2003.

[6] Olsson, I., Bunketorp, O., Carlsson G.,Gustafsson, C., Planath, I., Norin, H., Ysander, L. "An In-Depth Study of Neck Injuries in Rear End Collisions", 1990 International Conference on the Biomechanics of Impacts, Lyon, France, September, 1990.

[7] Svensson, M., Lovsund, P., Haland, Y., Larsson, S. The Influence of Seat-Back and Head-Restraint Properties on the Head-Neck Motion during Rear-Impact, 1993 International Conference on the Biomechanics of Impacts, Eindhoven, Netherlands, September, 1993.

[8] Voo L, McGee B, Merkle A, Kleinberger M, and Kuppa S. Performance of seats with active head restraints in rear impacts. 20th Enhanced Safety of Vehicles Conference, Paper No. 07-0041, Lyon, France, June, 2007.

[9] Voo LM, Merkle A, Wright J, and Kleinberger M: "Effect of Head-Restraint Rigidity on Whiplash Injury Risk," Proc Rollover, Side and Rear Impact (SP-1880), Paper #2004-01-0332, 2004_SAE World Congress, Detroit, MI, March 8 - 11, 2004.

APPENDIX

Seatback Rotations

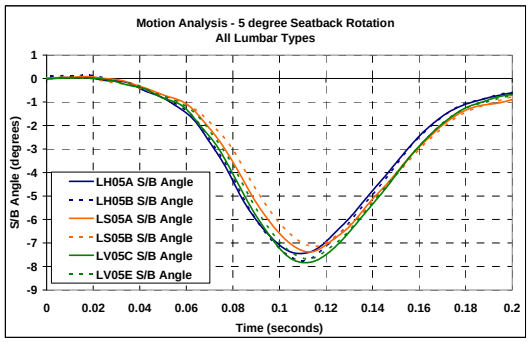

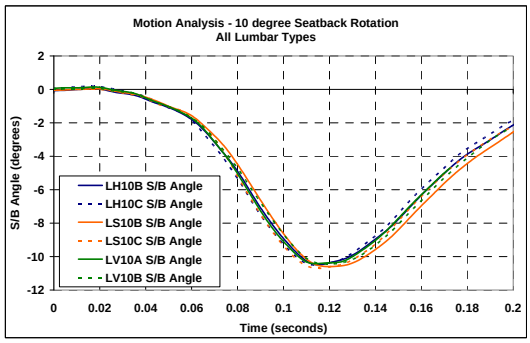

Angular Rate Sensor and Motion Analysis

Test ID	Gyro Head Rotation (degrees)	MA Head Rotation [degrees]	Gyro Torso Rotation (degrees)	MA Torso Rotation [degrees]	Gyro H wrt T Rotation (degees)	MA H wrt T Rotation [degrees]
LH05A	18.15	18.55	10.76	11.67	10.06	9.51
LH05B	18.88	19.17	11.92	13.02	9.81	8.92
LH10B	22.55	23.64	16.65	17.58	9.67	9.60
LH10C	22.22	22.95	17.72	19.14	8.68	8.01
LH15B	27.48	28.23	23.57	24.46	9.11	8.88
LH15C	23.69	24.37	21.74	22.92	6.14	5.51
LS05A	20.81	21.48	11.29	12.26	12.23	11.83
LS05B	17.75	18.76	10.32	11.14	9.87	9.99
LS10B	25.30	25.19	19.06	19.84	10.50	9.51
LS10C	18.30	18.99	18.05	18.75	5.91	5.87
LS15B	26.98	27.74	22.02	23.14	10.14	9.62
LS15C	28.85	29.93	23.89	25.02	9.29	8.99
LV05C	20.44	20.99	12.12	13.16	11.01	10.31
LV05E	19.69	20.36	12.00	12.79	10.47	10.22
LV10A	24.33	25.32	18.40	19.00	9.65	10.01
LV10B	24.32	24.90	19.52	20.91	9.02	8.50
LV15A	27.38	27.96	23.52	24.60	8.72	8.10
LV15B	28.26	28.92	23.38	24.40	8.44	7.86

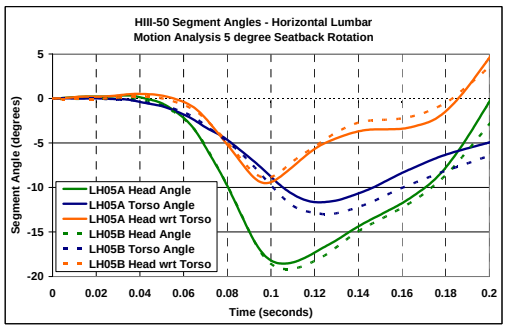

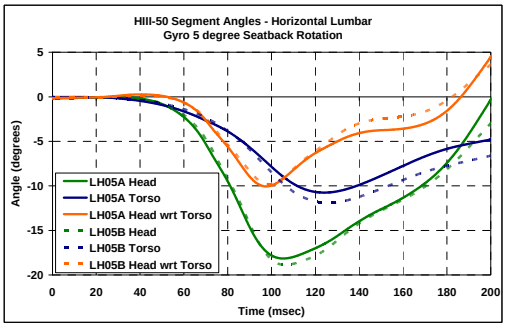

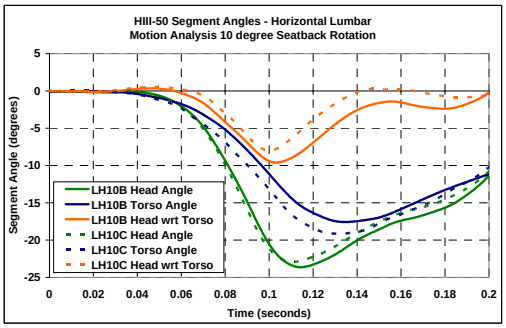

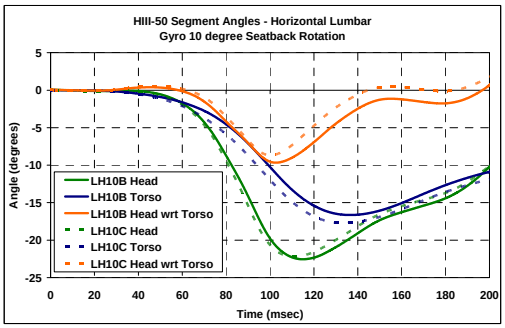

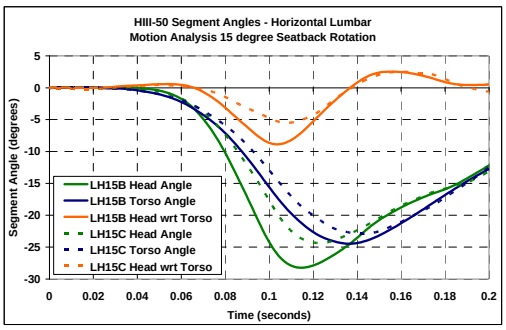

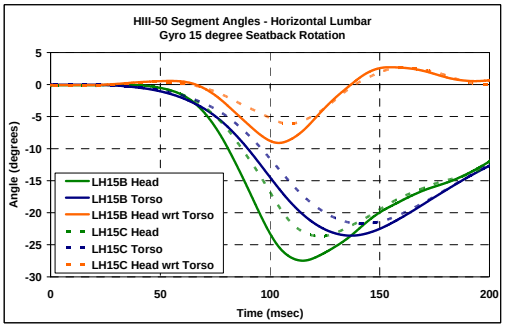

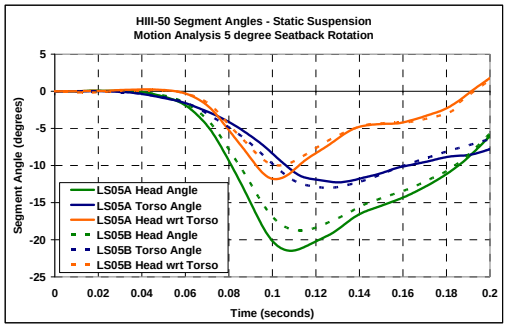
HIII-50 Segment Angles - Static Suspension
Motion Analysis 5 degree Seatback Rotation
Segment Angle (degrees)
Time (seconds)
LS05A Head Angle
LS05A Torso Angle
LS05A Head wrt Torso
LS05B Head Angle
LS05B Torso Angle
LS05B Head wrt Torso

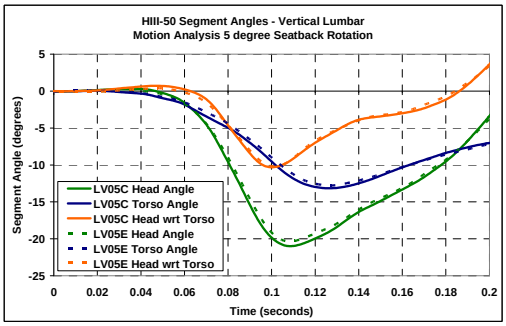
HIII-50 Segment Angles - Vertical Lumbar
Motion Analysis 5 degree Seatback Rotation
Segment Angle (degrees)
Time (seconds)
LV05C Head Angle
LV05C Torso Angle
LV05C Head wrt Torso
LV05E Head Angle
LV05E Torso Angle
LV05E Head wrt Torso

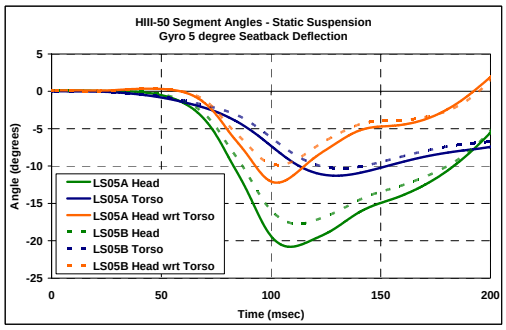
HIII-50 Segment Angles - Static Suspension
Gyro 5 degree Seatback Deflection
Angle (degrees)
Time (msec)
LS05A Head
LS05A Torso
LS05A Head wrt Torso
LS05B Head
LS05B Torso
LS05B Head wrt Torso

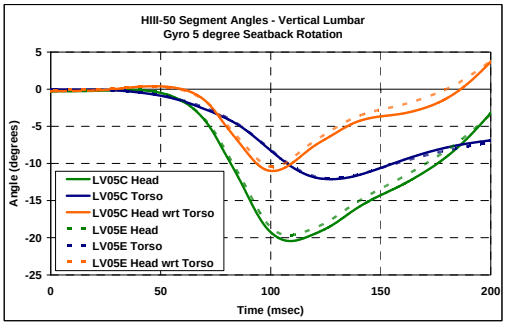
HIII-50 Segment Angles - Vertical Lumbar
Gyro 5 degree Seatback Rotation
Angle (degrees)
Time (msec)
LV05C Head
LV05C Torso
LV05C Head wrt Torso
LV05E Head
LV05E Torso
LV05E Head wrt Torso

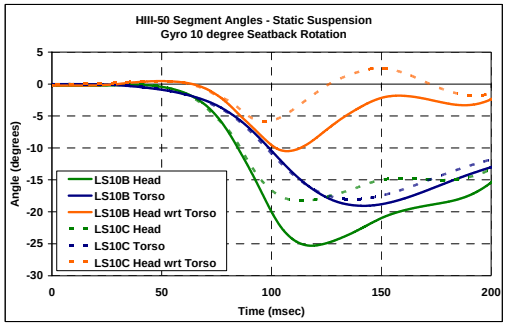
HIII-50 Segment Angles - Static Suspension
Gyro 10 degree Seatback Rotation
Angle (degrees)
Time (msec)
LS10B Head
LS10B Torso
LS10B Head wrt Torso
LS10C Head
LS10C Torso
LS10C Head wrt Torso

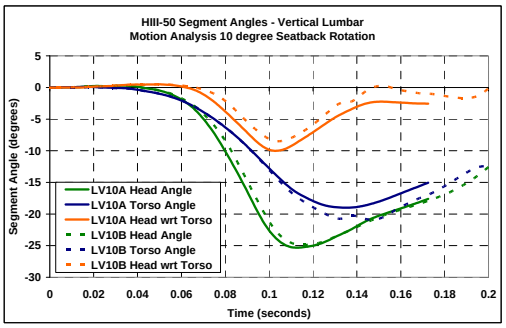
HIII-50 Segment Angles - Vertical Lumbar
Motion Analysis 10 degree Seatback Rotation
Segment Angle (degrees)
Time (seconds)
LV10A Head Angle
LV10A Torso Angle
LV10A Head wrt Torso
LV10B Head Angle
LV10B Torso Angle
LV10B Head wrt Torso

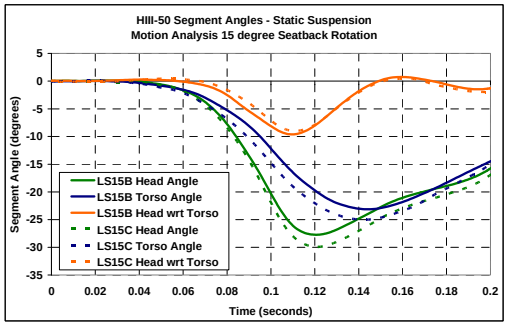
HIII-50 Segment Angles - Static Suspension
Motion Analysis 15 degree Seatback Rotation
Segment Angle (degrees)
Time (seconds)
LS15B Head Angle
LS15B Torso Angle
LS15B Head wrt Torso
LS15C Head Angle
LS15C Torso Angle
LS15C Head wrt Torso

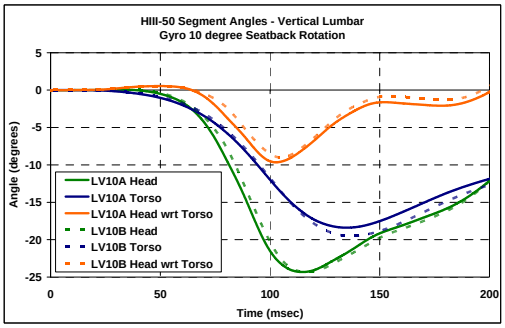
HIII-50 Segment Angles - Vertical Lumbar
Gyro 10 degree Seatback Rotation
Angle (degrees)
Time (msec)
LV10A Head
LV10A Torso
LV10A Head wrt Torso
LV10B Head
LV10B Torso
LV10B Head wrt Torso

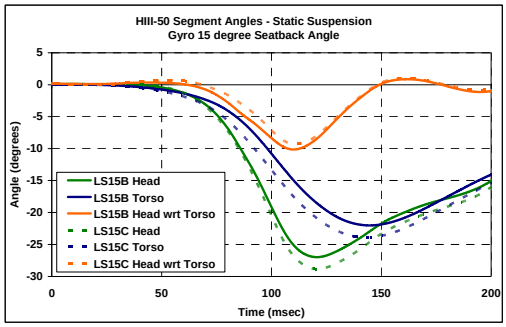
HIII-50 Segment Angles - Static Suspension
Gyro 15 degree Seatback Angle
Angle (degrees)
Time (msec)
LS15B Head
LS15B Torso
LS15B Head wrt Torso
LS15C Head
LS15C Torso
LS15C Head wrt Torso

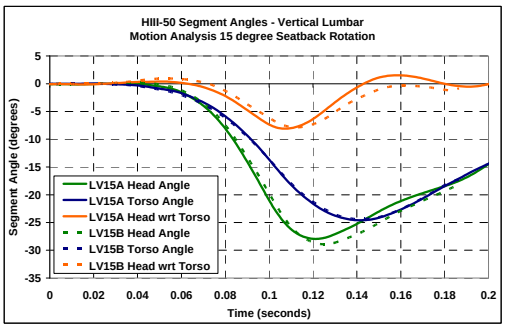
HIII-50 Segment Angles - Vertical Lumbar
Motion Analysis 15 degree Seatback Rotation
Segment Angle (degrees)
Time (seconds)
LV15A Head Angle
LV15A Torso Angle
LV15A Head wrt Torso
LV15B Head Angle
LV15B Torso Angle
LV15B Head wrt Torso

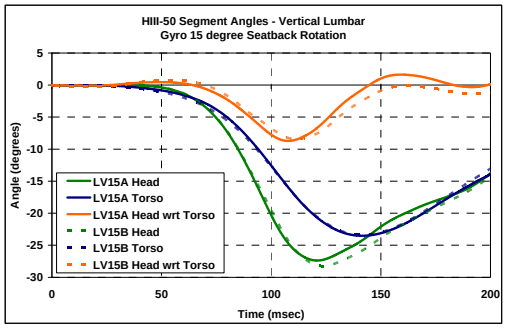

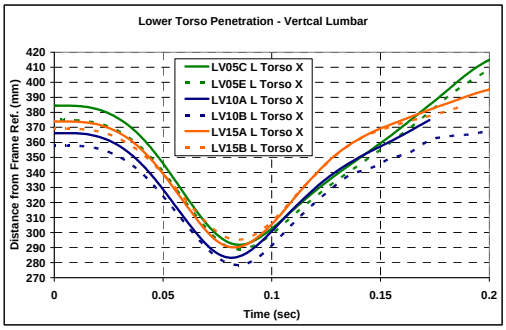
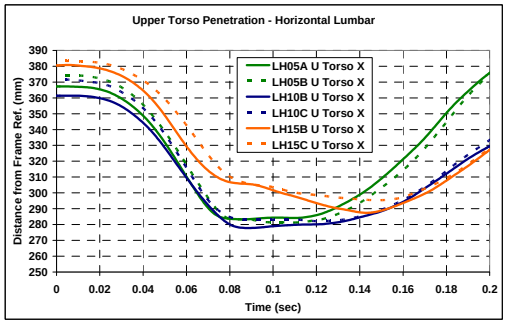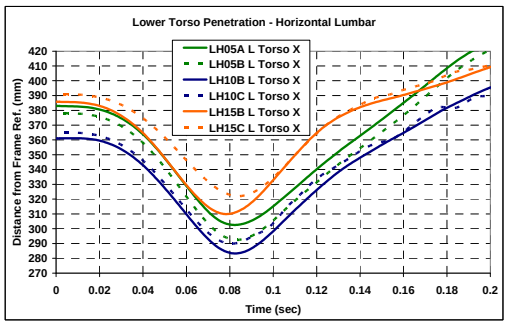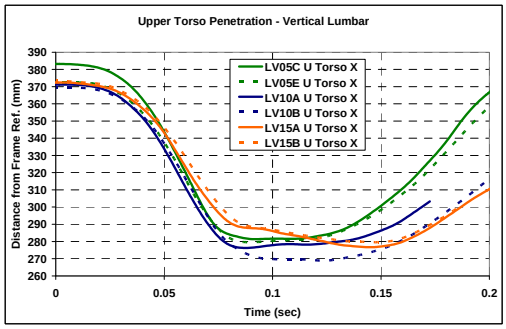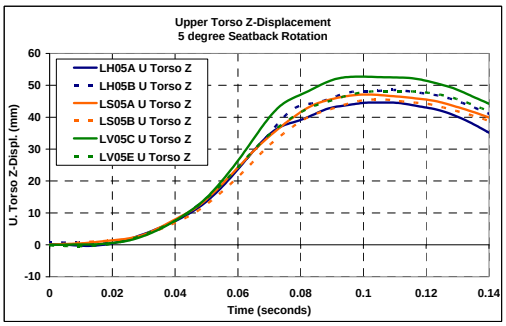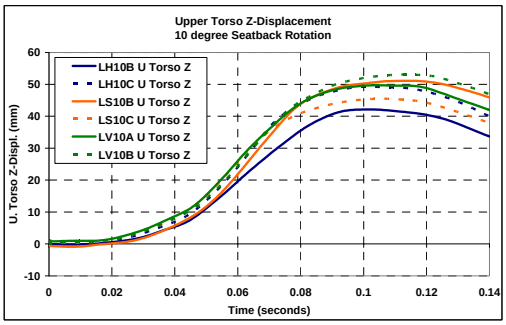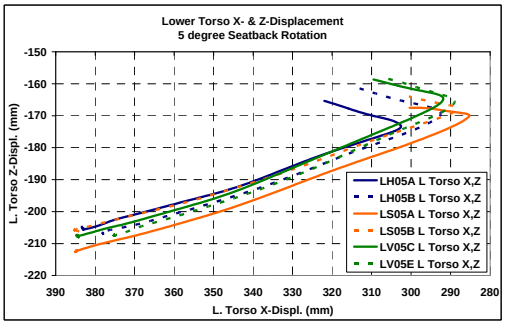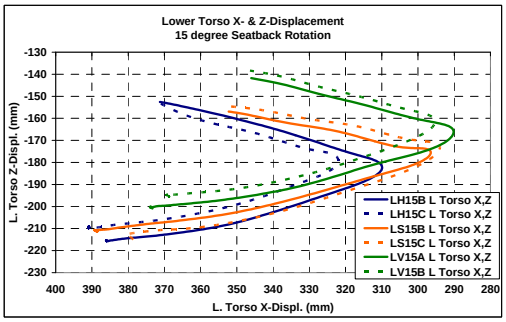
Torso Displacements